L. Wu, M. Akgul, Z. Ren, and C. T.-C. Nguyen, "Micromechanical disk array-composite for enhanced frequency stability against bias voltage fluctuations," *Proceedings*, IEEE Int. Ultrason., Ferroelect., Freq. Contr. Joint Symp., Prague, Czech Republic, July 21-25, 2013, pp. 547-550.

Micromechanical Disk Array for Enhanced Frequency Stability Against Bias Voltage Fluctuations

Lingqi Wu, Mehmet Akgul, Wei-Chang Li, Yang Lin, Zeying Ren, Tristan Rocheleau, and Clark T.-C. Nguyen
Department of EECS, University of California, Berkeley, CA, USA, Email: wulingqi@berkeley.edu

***Abstract*—A 215-MHz polysilicon capacitive-gap transduced micromechanical resonator array employing 50 mechanically coupled radial-contour mode disks—the largest such array yet fabricated and measured—has achieved 3.5× better frequency stability than single stand-alone disks against fluctuations in the dc bias voltage (V_P) normally applied across electrode-to-resonator gaps during device operation. The key to enhanced frequency stability is the electrode-to-resonator capacitance (C_o) generated by the parallel combination of input/output electrodes overlapping each resonator in the array that in turn reduces the efficacy of the bias voltage-controlled electrical stiffness. Here, a new equivalent circuit based on negative capacitance provides improved visualization that helps to identify methods to suppress electrical stiffness induced frequency variation. The circuit model indicates that the more resonators in an array, the smaller the frequency shift imposed by a given bias voltage change. Both modeling and measurement suggest that the most stable MEMS-based oscillators (e.g., against supply noise and acceleration) are ones that utilize mechanically-coupled arrays of resonators.**

***Keywords*—array, negative capacitance, electrical stiffness, micromechanical resonator, frequency stability, capacitive-gap transducer.**

I. Introduction

High-Q capacitive-gap transduced micromechanical resonators constructed via MEMS technology have recently taken center-stage among potential next generation timing and frequency reference devices that might satisfy present and future applications. Notably, oscillators referenced to very high Q capacitively transduced MEMS resonators have already made inroads into the low-end timing market, and research devices have been reported to satisfy GSM phase noise requirements [1] [2]. Meanwhile, such devices have also posted some impressively low acceleration sensitivities, with measured sensitivity vectors less than 0.5ppb/g [3].

Interestingly, theory predicts that the acceleration sensitivity of these devices should be even better than this, if not for frequency instability due to electrical stiffness [3]. Indeed, electrical stiffness is predicted to set lower limits on not only short-term stability, but long-term as well, especially when one considers frequency variations due to charging or temperature-induced geometric shifts [4].

Pursuant to circumventing electrical stiffness-based instability, this work introduces a more circuit design-friendly model that uses negative capacitance to capture the influence of electrical stiffness on device and circuit behavior. This new circuit model reveals that capacitive-gap transduced micromechanical resonators can offer better stability against electrical-stiffness-based frequency instability when used in large mechanically-coupled arrays. Measurements confirm that a 215-MHz 50-resonator disk array achieves a 3.5× enhancement in frequency stability against dc-bias voltage variation over a stand-alone single disk counterpart. The new equivalent circuit predicts the measurement data and its trends quite well, creating good confidence for using this circuit to guide new oscillator and filter designs that, depending on the application, can enhance or suppress electrical stiffness.

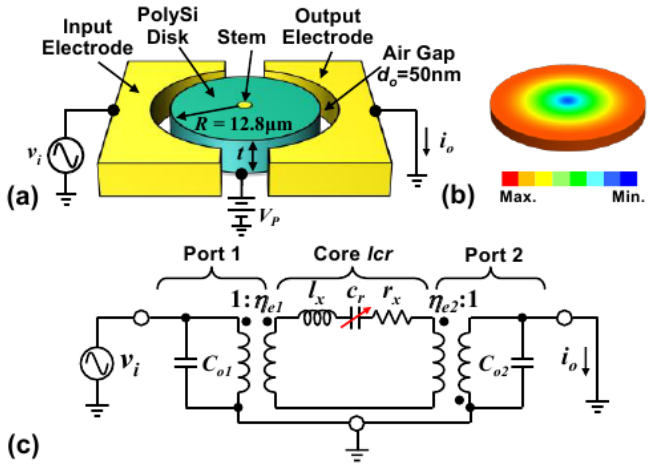

Fig. 1. (a) Schematic of a 215-MHz radial-contour mode polysilicon disk resonator in a two-port excitation and sensing configuration. (b) Radial-contour mode shape. (c) Classic equivalent electrical circuit for a capacitive gap micromechanical disk resonator with electrical stiffness lumped into the variable capacitance c_r.

II. Contour Mode Disk Resonator

Fig. 1(a) depicts a capacitive gap polysilicon contour mode disk resonator in a typical bias, excitation, and detection scheme. This device comprises a 2μm-thick (t=2μm) polysilicon disk supported by an anchored stem attached at the center of the disk and surrounded by two electrodes separated by a tiny 50nm air gap (d_o=50nm). The device is excited into resonance via a combination of a dc-bias voltage V_P applied to the conductive polysilicon resonant structure and an ac signal applied to the input electrode, which together induce a force at the frequency of v_i that drives the disk into a contour mode resonance with equal radial expansion and contraction around its perimeter, as shown in Fig. 1(b), when the frequency of v_i matches the resonance frequency. Once vibrating, the V_P-biased time varying capacitance between the disk and its output electrode generates an output current.

To conveniently model and simulate the behavior of this micromechanical disk resonator, [5] provided expressions for the element values of the electrical equivalent circuit shown in Fig. 1(c), which take the form

$$l_x = m_m,\ r_x = c_m,\ c_r = \frac{1}{k_m - k_e},\ \eta_{en} = \frac{V_P C_{on}}{d_o} \qquad (1)$$

where m_m, k_m, c_m, η_{en}, and C_{on} are the equivalent dynamic mass, mechanical stiffness, damping, electromechanical coupling factor, and electrode-to-resonator capacitance at corresponding ports, respectively. The electrical stiffness k_e models the frequency pulling effect of the force generated by time-varying changes in electric field strength as vibration changes the parallel-plate capacitive electrode-to-resonator gap and can be expressed as [6]

$$k_e = \frac{V_P^2 (C_{o1} + C_{o2})}{d_o^2} = \frac{V_P^2 \epsilon A}{d_o^3} \qquad (2)$$

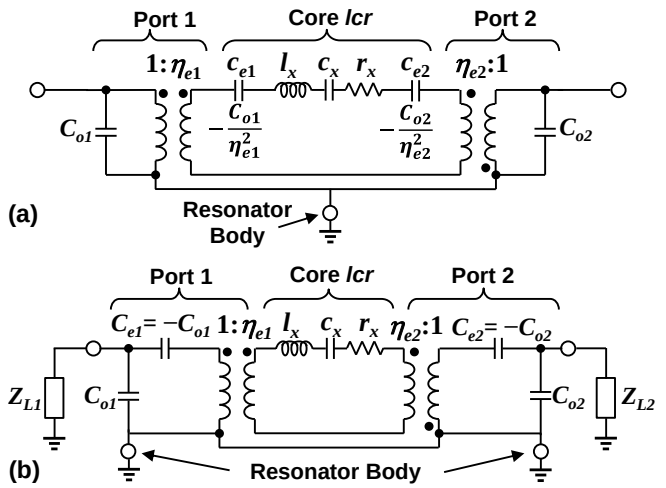

Fig. 2. Negative capacitance small-signal equivalent circuits for a two-port capacitive-gap micromechanical contour mode disk resonator: (a) Negative capacitance equivalent circuit with electrical stiffness separated from mechanical stiffness. (b) Negative capacitance equivalent circuit with electrical stiffness reflected through transformers to outside the core *lcr* loop.

where ϵ is the permittivity of the gap material (i.e., vacuum in this case) and A is the total overlap area between the resonator and its electrodes. Since the force generated by k_e is in phase with displacement and acts to accentuate motion, it acts against the mechanical spring restoring force, so subtracts from the mechanical stiffness, yielding a total resonator stiffness of $(k_m - k_e)$. Changes of any variables in k_e, such as dc-bias voltage noise, capacitance variation due to mechanical vibration, or charging induced bias voltage drift, can cause frequency stability issues for capacitive-gap MEMS resonators [7] [8].

The classic equivalent circuit in Fig. 1(c) models the influence of electrical stiffness on resonance frequency via the arrow through capacitor c_r (that indicates this capacitor is tunable) and by setting the value of c_r equal to $1/(k_m - k_e)$. Although this method for capturing electrical stiffness adequately predicts the resonance frequency, it does not convey clearly to a circuit designer the impact of electrical stiffness on the overall circuit performance. Modeling the electrical stiffness in this way in fact hides some very important capacitive-gap resonator behaviors when emplaced into certain circuits. This model also encourages designers to dismiss the impact of electrical stiffness, since many designers just neglect the k_e part in the value of c_r when drawing up equivalent circuits.

III. Negative Capacitance Equivalent Circuit

To remedy the above deficiencies, the circuit of Fig. 2(a) explicitly models the electrical stiffness contributed by each electrode-to-resonator gap as separate negative capacitors c_{en}, where n denotes the port. Using (1) and (2), c_{en} becomes

$$c_{en} = -\frac{1}{k_{en}} = -\frac{d_o^2}{V_P^2 C_{on}} = -\frac{C_{on}}{\eta_{en}^2} \tag{3}$$

Here, c_{en} entirely captures the electrical stiffness, allowing c_x in Fig. 2(a) to represent the pure mechanical stiffness. Further reflecting the negative capacitors c_{en} through the transformers on both sides to outside the core *lcr* loop yields C_{en} in the circuit of Fig. 2(b) as follows:

$$C_{en} = \eta_{en}^2 c_{en} = -C_{on} \tag{4}$$

where the physical shunt electrode-to-resonator capacitors C_{on} are now matched by negative capacitors with identical values. This new circuit reveals the potential for cancellation of the C_{on}'s in certain circuit configurations, which where possible, would remove entirely frequency changes induced by electrical stiffness, thereby stabilizing the frequency against all variables in (2)—something highly desirable for oscillator applications that require very high frequency stability.

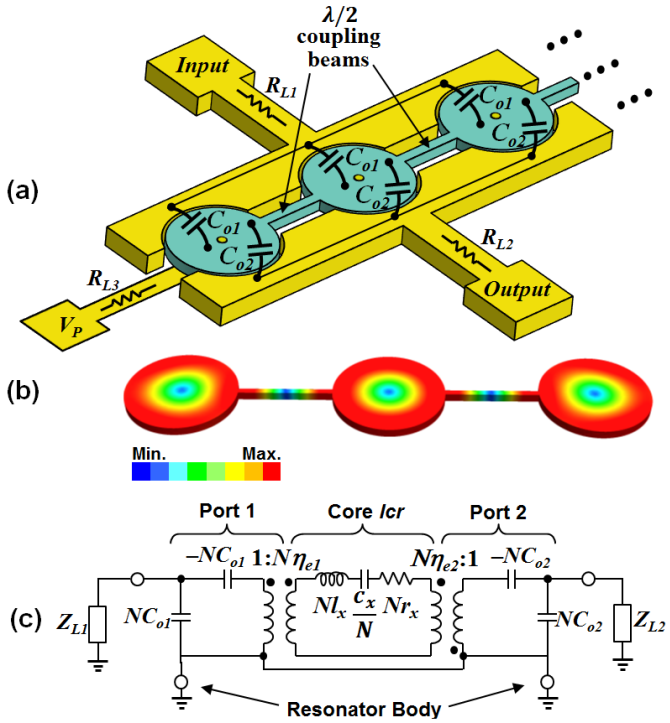

Fig. 3. (a) Schematic of a disk array-composite resonator with disks linked by λ/2 coupling beams to enforce in phase vibration of each individual resonator. (b) Simulated modal depiction of a 3-resonator disk array with all disks vibrating in phase in radial-contour shapes. (c) Negative capacitance equivalent circuit of a disk array-composite with *N* resonators based on element values of the single resonator equivalent circuit in Fig. 2(b)

Pursuant to determining which circuit configurations best promote k_e cancellation, Fig. 2(b) adds load impedances Z_{Ln}. In order for C_{on} to negate the electrical stiffness represented by $-C_{on}$, approximately same amount of current should flow through C_{on} and $-C_{on}$, which indicates that C_{on} should pass most of the current flowing into the parallel combination of C_{on} and Z_{Ln}. In other words, the impedance of Z_{Ln} should be much larger than that of C_{on}, or

$$|Z_{Ln}| \gg \frac{1}{\omega_o C_{on}} \tag{5}$$

From (5), to reduce electrical stiffness, both Z_{Ln} and C_{on} should be large. If Z_{Ln} has no reactive component, operation at high frequency also suppresses electrical stiffness. To address cases where a resonator might be used with reconfigurable drive and sense circuits that present non-constant loads, and to reap the motional resistance and power handling advantages of arrays, this work focuses on coupled-array-based methods to increase C_{on} towards better frequency stability against changes in electrical stiffness.

IV. Micromechanical Disk Array

Fig. 3(a) presents a micromechanical disk array-composite constructed by mechanically linking individual disk resonators via half-wavelength coupling beams. Here, coupling of resonators yields a coupled multi-mode system, where at each mode, all resonators vibrate at precisely the same frequency [9], allowing their outputs to be combined to boost input and output currents, thereby decreasing the motional resistance and increasing power handling. As first demonstrated in [1], the use of half-wavelength couplers both insures that all resonators vibrate in phase, as shown in Fig. 3(b); and spreads the mode

TABLE I. COMPARISON OF EQUIVALENT CIRCUIT ELEMENT VALUES FOR A 50-RESONATOR DISK ARRAY AND A SINGLE DISK RESONATOR

Parameters	Single Disk Resonator	Disk Array with N =50
C_{on} (fF)	9	451
η_{en}	1.58×10^{-6}	7.91×10^{-5}
l_x (H)	1.81×10^{-12}	9.03×10^{-11}
r_x (Ω)	1.17×10^{-7}	5.85×10^{-6}
c_x (F)	3.29×10^{-7}	6.59×10^{-9}

frequencies apart, making it easier to select a specific mode (when only one is wanted, e.g., in an oscillator application) by proper electrode phasing. Of course, this coupled array strategy not only produces a larger total output current and smaller motional resistance [10], but also attains much larger electrode-to-resonator overlap capacitors C_{on}, and thus reduces the electrical stiffness and its associated instability, according to (5).

For a disk array with N mechanically coupled disk resonators, the stiffness k_m, mass m_m, damping c_m, electromechanical coupling factor η_{en}, and electrode-to-resonator overlap capacitance C_{on} are all N times larger than for a single disk resonator. Thus, simple multiplication or division by N is all that is needed to derive coupled array equivalent circuit element values from those of a single disk resonator, as shown in Fig. 3(c). Note that although the electrical stiffness goes up by N according to (2), so does the mechanical stiffness, so their ratio k_e/k_m remains the same and the fundamental efficacy by which k_e pulls the frequency, as governed by

$$f_o = f_{nom}\sqrt{1 - \frac{k_e}{k_m}} \qquad (6)$$

does not increase (where f_o is the resonance frequency and f_{nom} is the nominal resonance frequency with no electrical stiffness). Instead, with C_{on} presenting a much smaller impedance, more current flows through C_{on} than Z_{Ln}, allowing it to cancel more of C_{en}, thereby negating the electrical stiffness induced frequency instability via circuit interaction.

TABLE I summarizes the equivalent circuit element values for a 215-MHz 50-nm-gap disk array using 50 resonators (with Q=20,000 and V_P=10V) and compares them with that of a stand-alone single disk resonator. With a 451fF electrode-to-resonator overlap capacitance much larger than the 9fF of a single disk, the 50-resonator array should greatly suppress electrical stiffness induced frequency instability.

V. FABRICATION PROCESS

The fabrication process for the all-polysilicon contour mode disk resonator arrays of this work deviates from previous ones, such as that of [11], in that it does not use self-aligned peg-stem anchors and it employs chemical mechanical polishing (CMP) to remove electrode overhangs. The process begins with film depositions and etches identical to those of [11] to achieve the substrate isolation layer, polysilicon interconnects, and the bottom sacrificial layer. At this point, unlike previous self-aligned processes, a mask is used to define, pattern, and etch stem anchor holes into the bottom sacrificial oxide, followed by a 2-μm LPCVD in-situ doped polysilicon film that fills the holes to form the stems and serves as the resonator structural material. Here, an AMSL300 DUV Stepper is used to realize very precise alignment, with less than 100nm error—good enough to achieve Q's comparable to those of devices with self-aligned stems.

After depositing an oxide hard mask over the structural polysilicon, disk devices and coupling links are patterned and

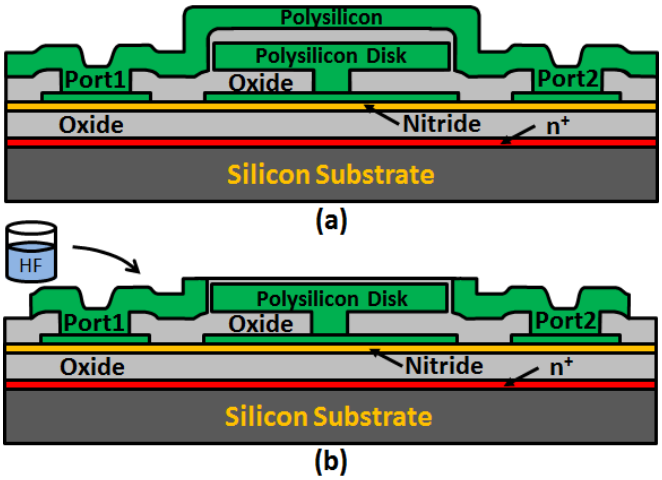

Fig. 4. Cross-sections showing the last few steps in the fabrication process for a 215-MHz all-polysilicon disk resonators with CMPed electrodes.

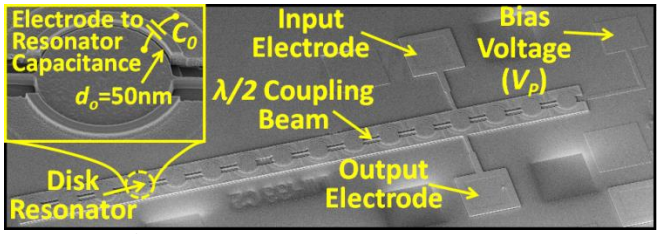

Fig. 5. SEM of a 215-MHZ 50nm capacitive-gap transduced contour mode disk array employing 16 mechanically coupled resonators.

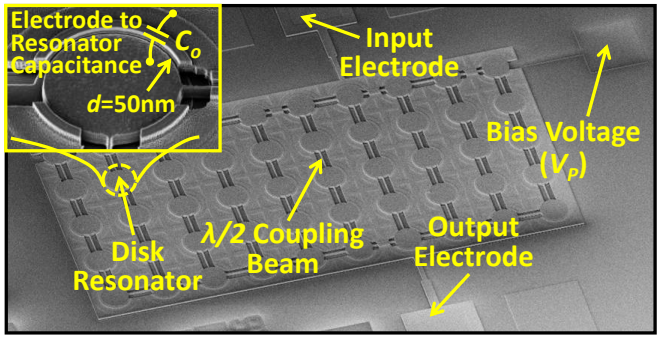

Fig. 6. SEM of a 215-MHZ 50nm capacitive-gap transduced contour mode disk array employing 50 mechanically coupled resonators.

etched as before, the gap-defining sacrificial sidewall oxide spacer is deposited, electrode to interconnect contact vias are etched, and the polysilicon electrode material LPCVD'ed 3-μm thick, all to yield the cross-section of Fig. 4(a). At this point, the process again deviates from that of [11] in that before patterning and etching the electrodes, the top polysilicon is first CMP'ed down to the hard mask. This step removes the electrode overhangs of Fig. 4(a), achieving the cross section of Fig. 4(b), and in the process greatly increasing the pull-in voltage of these devices, where contact between the disk and the electrode overhang is often the first to occur when dc-bias voltages increase. As before, devices are released in 49 wt. % hydrofluoric acid for ~40min.

Fig. 5 and Fig. 6 present SEMs of fabricated 215-MHz 50-nm capacitive-gap transduced half-wavelength-coupled disk arrays employing 16 and 50 resonators, respectively, in straight line and rectangular placement configurations.

VI. EXPERIMENTAL RESULTS

To gauge the degree to which arraying enhances frequency stability against dc-bias voltage changes, measured plots of frequency versus dc-bias voltage are in order, for both mechanically coupled disk array-composite resonators using various numbers of resonators, as well as for a single stand-alone disk for comparison. To this end, measurements were made under a

2μtorr vacuum environment in a Lakeshore FWPX vacuum probe station and using an Agilent E5071C network analyzer in the direct two-port excitation and sensing scheme depicted in Fig. 1(a). Fig. 7 presents measured curves that clearly show a shrinking frequency dependence on dc-bias voltage as the number of resonators used in an array increases. In particular, the 50-resonator 215-MHz disk array experiences a 20ppm frequency change when V_P varies over a 7V span, from 2V to 9V, 3.5× smaller than the 70ppm of a stand-alone device.

To confirm the validity of the negative capacitance equivalent circuit of Fig. 3(c), simulated plots using this circuit are also included in Fig. 7, showing very good agreement between theory and measurement. These simulations assume the load impedance Z_{Ln} derives from a combination of series trace resistance R_{L1} and R_{L2} from input/output electrode leads, as well as similar lead resistance R_{L3} from the V_P port, all shown in Fig. 3(a). Since probe coax and bond pad capacitance are nulled by calibration, the Z_{Ln} in these measurements is mainly resistive. It should be noted that the total equivalent load resistance $R_{Ln,tot}$ of a disk array in this work is generally larger than that of a single resonator and actually increases with the number of disks in the array. This comes about because, at least in the current layout, the distance between the V_P pad and the furthest resonator increases as the number of resonators increases, as seen from Fig. 5, resulting in a corresponding increase in series resistance R_{L3}. TABLE II summarizes overlap capacitance and equivalent load resistance values for disk arrays with N=1, 8, 16, and 50, clearly showing larger values as the number of resonators increases, at least for straight line arrays with N=8 and N=16, like that of Fig. 5. The series resistance of the 50-resonator array depicted in TABLE II is actually smaller than those of the 8- and 16-resonator ones, since its layout uses a rectangular or matrix topology, rather than a straight line, so the average distance of its resonators from its V_P pad ends up being smaller.

According to (5), increases in load resistance like those in TABLE II should also contribute to an overall nulling of the electrical stiffness, and thereby enhance frequency stability against dc-bias voltage fluctuations. Indeed, as the number of array resonators increases, electrical stiffness erodes due to increases in both electrode-to-resonator overlap capacitance and load resistance—a double whammy effect perfectly predicted by the negative capacitance equivalent circuit.

VII. Conclusions

The 50-resonator capacitive-gap transduced micromechanical disk array demonstrated here is the largest such array yet fabricated and measured and enables a mere 20ppm frequency change over a 7V dc-bias voltage variation—a 3.5× reduction over a single stand-alone disk resonator counterpart. That the new negative capacitance equivalent circuit model introduced perfectly predicts this phenomenon, while also aiding circuit visualization, bodes well for its continued use in future resonator circuits for which tailored electrical stiffness strengths are desired. Indeed, the demonstrated stability enhancing attributes of mechanically-coupled arrays that make them less vulnerable to dc-bias voltage noise, dielectric charging, and external vibrations, together with already demonstrated array-derived reductions in the standard deviation of array resonance frequency [12], present strong cases for a more prevalent use of arrays in next generation MEMS-based frequency reference devices.

Acknowledgment: This work was supported by the DARPA CSSA program.

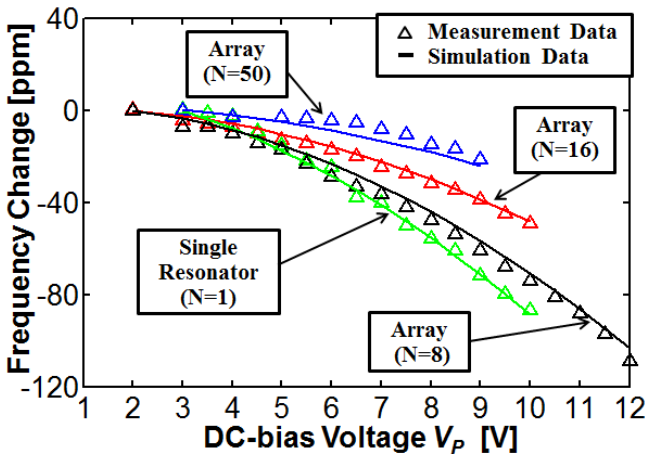

Fig. 7. Measured curves of resonance frequency versus dc-bias voltage V_P plotted against simulation using negative capacitance equivalent circuit models for disk arrays with N=1, N=8, N=16, and N=50.

TABLE II. *N*-Resonator Disk Array Parameters

Resonator Number (N)	Overlap Capacitance C_{on} [fF]	$R_{Ln,tot}$ [kΩ]
1	9	1.56
8	72	4.04
16	144	5.24
50	451	2.92

References

[1] Y.-W. Lin, S.-S. Li, Z. Ren and C. T.-C. Nguyen, "Low phase noise array-composite micromechanical wine-glass disk oscillator," in *Technical Digest, IEEE, Int. Electron Device Mtg.*, Washington, DC, Dec. 5-7, 2005.

[2] V. Kaajakari *et al.*, "Square-extensional mode single-crystal silicon micromechanical resonator for low-phase-noise oscillator application," *IEEE Electron Device Letters*, vol. 25, no. 4, pp. 173-175, 2004.

[3] T. L. Naing *et al.*, "vibration-insensitive 61-MHz micromechanical disk reference oscillator," in *IEEE Int. Frequency Control Symposium*, Baltimore, Maryland, May 22-24, 2012.

[4] V. Kaajakari, J. K. Koskinen and T. Mattila, "Phase noise in capacitively coupled micromechanical oscillators," *IEEE Transactions on Ultrasonics, Ferroelectric, and Frequency Control*, vol. 52, no. 12, pp. 2322-2331, 2005.

[5] F. D. Bannon, J. R. Clark and C. T.-C. Nguyen, "High-Q HF micromechanical filters," *IEEE Journal of Solid-State Circuits*, vol. 35, no. 4, pp. 512-526, 2000.

[6] H. C. Nathanson, W. E. Newell, R. A. Wickstrom and J. R. Davis JR., "The resonant gate transistor," *IEEE Transactions on Electron Devices*, vol. 14, no. 3, pp. 117-133, Mar. 1967.

[7] M. Agarwal *et al.*, "Effects of mechanical vibrations and bias voltage noise on phase noise of MEMS resonator based oscillators," in *19th IEEE Int. Micro Electro Mechanical System Conf.*, Istanbul, Turkey,, Jan. 22-26, 2006.

[8] G. Bahl *et al.*, "Model and observations of dielectric charge in thermally oxidized silicon resonators," *Journal of Microelectromechanical Systems*, vol. 19, no. 1, pp. 162-174, 2010.

[9] R. A. Johnson, Mechanical Filters in Electronics, New York: Wiley, 1983.

[10] M. U. Demirci and C. T.-C. Nguyen, "Mechanically corner-coupled square microresonator array for reduced series motional resistance," *Journal of Microelectromechanical Systems*, vol. 15, no. 6, Dec. 2006.

[11] J. Wang, Z. Ren and C. T.-C. Nguyen, "1.156-GHz self-aligned vibrating micromechanical disk resonator," *IEEE Transactions on Ultrasonics, Ferroelectrics, and Frequency Control*, vol. 51, no. 12, pp. 1607-1628, Dec. 2004.

[12] Y. Lin *et al.*, "Enhancement of micromechanical resonator manufacturing precision via mechanically-coupled arraying," in *IEEE Int. Frequency Control Symp.*, Besancon, France, Apr. 20-24, 2009.